

Multi-band character revealed from Weak-antilocalization effect in Platinum thin films

Subhadip Jana,^{1,2,*} T. Senapati,^{3,2} K. Senapati,^{3,2} and D. Samal^{1,2,†}

¹*Institute of Physics, Bhubaneswar, 751005, India*

²*Homi Bhabha National Institute, AnushaktiNagar, Mumbai, 400094, India*

³*School of Physical Sciences, National Institute of Science Education and Research, Bhubaneswar, 752050, India*

Platinum (Pt) has been very much used for spin-charge conversion in spintronics research due to its large intrinsic spin-orbit interaction. Magnetoconductance originated from weak-antilocalization effect in quantum interference regime is used as a powerful tool to obtain the microscopic information of spin-orbit interaction and coherence phase breaking scattering process among itinerant electrons. To acquire the knowledge of different types of scattering processes, we have performed magnetoconductance study on Pt thin films which manifests multi-band (multi-channel) conduction. An extensive analysis of quantum interference originated weak-antilocalization effect reveals the existence of strong (weak) inter-band scattering between two similar (different) orbitals. Coherence phase breaking lengths (l_ϕ) and their temperature dependence are found to be significantly different for these two conducting bands. The observed effects are consistent with theoretical predication that there exist three Fermi-sheets with one s and two d orbital character. This study provides the evidence of two independent non-similar conducting channels and presence of anisotropic spin-orbit interaction along with e - e correlation in Pt thin films.

I. INTRODUCTION

Gaining control over electron spin degree of freedom is very much desirable in the field of spintronic research^{1,2}. In recent days, spin-orbit interaction (SOI) has been found to provide promising strategy for electrical manipulation spin/magnetism in spintronic devices³⁻⁶. This includes the creation of spin current from transverse charge current effect (SHE)⁷⁻⁹, and the exertion of a torque on a local magnetization from electrical current by spin-orbit torque effect¹⁰⁻¹³. At a microscopic level, the asymmetric spin dependent electron scattering induced by SOI lies at the heart of the above phenomena^{14,15}. Besides, a broader implication of SOI is realized in the design of topological materials with their potential use in low energy dissipation and faster magnetization switching¹⁶⁻¹⁹. Materials with high Z element (Z is atomic number) are ideal candidates to look for spin-orbit interaction induced phenomena (SOI strength $\propto Z^4$ ²⁰). In particular, $5d$ transition metal Pt has drawn lot of attention for spin-charge conversions and spin-torque effect in Pt/magnetic layer based heterostructures due to its intrinsic high SOI²¹⁻²⁴. Further, the observation of inverse spin hall effect (ISHE) (reverse process of SHE, *i.e.* creation of charge current from transverse spin current) in $\text{Ni}_{81}\text{Fe}_{19}/\text{Pt}$ and in Pt wire at room temperature provided an effective way to detect spin current^{25,26}. In view of the extensive use of Pt in spintronics owing to its chemical inertness, easy fabrication of device and most importantly strong intrinsic spin-orbit interaction, it is important to have a comprehensive understanding of the effect of spin-orbit interaction on electronic transport in bare metallic Pt thin films.

Quantum interference originated weak-localization (WL) or weak-antilocalization (WAL) effect is very much sensitive to the spin-orbit interaction (SOI) scattering process in conducting systems²⁷. In real system, any type of deviation from perfect crystalline structure

acts as a source of scattering potential for itinerant electrons. Scattered electrons propagating along time-reversed, identical self-intersecting trajectories known as “Cooperon loop” (CL)^{28,29} interfere constructively/ destructively to give rise to suppression (WL)/ enhancement (WAL) of conductivity. Experimentally, WL/WAL is usually determined from conductance correction to classical Drude conductivity at low temperature and in presence of external magnetic field. The interference correction tends to vanish for most of trajectories after averaging over the random scattering potentials, except for those scattered electrons which propagate in CL.

The application of uniform external magnetic field breaks the time reversal symmetry required for the interference effect and induces an additional relative phase shift (due to enclose magnetic flux) between the two electrons traversing CL. This effect suppress constructive/destructive interference, as a result conductance gets enhanced (positive)/decrease (negative) with application of magnetic field in the WL/WAL regime^{30,31}. Therefore, variation of magnetoconductance is used as a sensitive probe to detect quantum interference effect. Traditionally, the manifestation of WAL has been attributed to SOI in material. In order for WAL to occur, it is crucial to have a π phase shift between two electron trajectories. The rotation of spin $1/2$ particle by 4π is equivalent to the identity operation. However, for Pt thin films 2π rotation of itinerant electron spin induced by SOI gives rise to π phase shift resulting in WAL effect^{32,33}.

In this work, we have carried out an indepth magnetotransport study to examine the underlying SOI scattering of itinerant electrons from WAL effect in Pt thin films. It has been realized that SOI scattering strength (proportional to the characteristic spin-orbit magnetic field ($B_{so} \sim 2$ T)) is very much stronger than coherent phase breaking scattering strength ($B_\phi \sim 0.004$ T at 2 K). The corresponding B_{so} and B_ϕ are extracted by using Hikami-Larkin-Nagaoka equation (Eq.7). Fur-

ther, it has been found that the single conduction channel can not be fitted well with experimental data, rather two independent conduction channels need to be considered to reconcile with experimental data. To get more information about channels and their orbital symmetry, we examined temperature dependent behavior of B_ϕ . It is found that $B_\phi^1(T)$ for one channel exhibits prominent temperature dependence whereas $B_\phi^2(T)$ corresponding to other channel shows weak temperature dependence. The observed difference in the temperature variation of $B_\phi^1(T)$ and $B_\phi^2(T)$ are attributed to two conducting channels made of orbitals with different symmetry. The band originated from more symmetric orbitals are less sensitive to disorder whereas the band originated from anisotropic orbitals are more sensitive to disorder and it is reflected in temperature dependent $B_\phi^1(T), B_\phi^2(T)$. The observed effects are consistent with theoretical predication that there exist three Fermi-sheets (FS) with one s and two d orbital character^{34–36}. This study provides the evidence of two independent nonsimilar conducting channels (one channel is made of s orbital FS and other is originated from combining two d orbital FS (illustrated in Fig.9)) and presence of anisotropic spin-orbit interaction along with e - e correlation in Pt thin films.

II. Experiment

Platinum thin films were grown on Si/SiO₂ substrates using DC magnetron sputtering at room temperature with a base pressure 5×10^{-8} mBar. Before deposition, photolithography patterning with a Hall bar geometry was done with a mask aligner MDA-400M-N on 5×5 mm² substrates. The thickness variation of Pt layer was achieved from a single deposition-run by rotating substrate plate holder. The structural characterization was carried out using a high-resolution X-ray diffractometer. The films were found to be polycrystalline with grains mainly grown/oriented on (111) plane. The thickness of the films was determined to be 16 nm and 23 nm with a roughness about 3 Å from X-ray reflectivity (XRR) measurement. The magneto transport measurements were performed in a Cryogenic physical property measurement system (PPMS) with magnetic fields applied parallel and perpendicular to the film surface. We used Keithley 6221 as the current source and a Keithley 2182A nano voltmeter for better data resolution.

III. Resistivity at low temperature

The temperature dependent resistivity (ρ) for 16, 23 nm thick films (Fig.1) exhibits positive temperature coefficient ($\frac{d\rho}{dT} > 0$) above 6 K indicating metallic character. Moreover, in the intermediate temperature range $15 \text{ K} < T < 26 \text{ K}$, the resistivity follows quadratic temperature dependence which is attributed to e - e coulomb

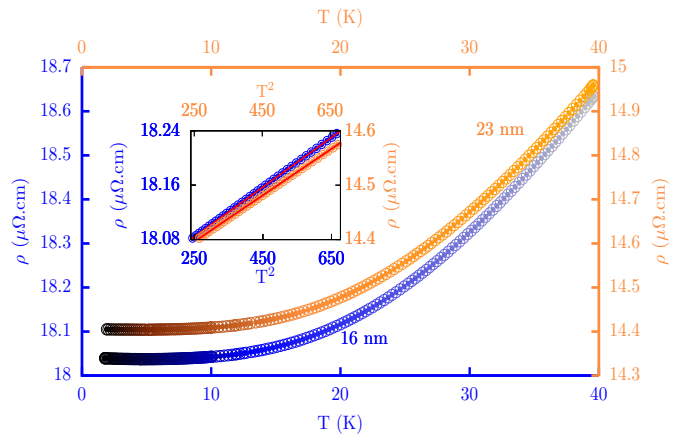


FIG. 1. Resistivity $\rho(T)$ vs T plot for Pt 16 nm (blue color) and 23 nm (orange color) films, darken color at low temperature indicates quantum interference regime. EEI originated $\rho(T) \propto T^2$ in the temperature range $15 \text{ K} < T < 26 \text{ K}$ is illustrated in inset (solid red color lines represent fitting of Eq.(1)).

interaction (EEI)^{37–39} and is shown in inset of Fig.1. Experimental data in the range temperature $15 \text{ K} < T < 26 \text{ K}$ the fits well with Eq.(1),

$$\rho(T) = \rho_0 + AT^2, \quad (1)$$

where ρ_0 is residual resistivity and A accounts for EEI contribution. From fitting, we obtain A equal to $3.6 \times 10^{-4} \mu\Omega\text{cm.K}^{-2}$ and $3.36 \times 10^{-4} \mu\Omega\text{cm.K}^{-2}$ for 16 nm and 23 nm thick films respectively. The obtained value of A is higher for 16 nm film as compared to 23 nm and it is consistent with theory that $A \propto E_F^{-2} \propto (m^*)^2$, where E_F and m^* are Fermi energy, effective mass of electron respectively⁴⁰. The extracted values of A are slightly higher than the reported value of ($A \sim 10^{-5} \mu\Omega\text{cm.K}^{-2}$) for bulk Pt³⁹ which could be due to reduction of system dimension.

In low temperature regime ($2 \text{ K} < T < 6 \text{ K}$), $\rho(T)$ exhibits an upturn which is attributed to the combined effect of quantum interference (WL/WAL) and EEI correction in quasi 2D limit. This regime is denoted by dark color shed in Fig.1 and it is discussed in Sec.IV in terms of sheet conductance correction.

IV. Signature of WAL Effect from Temperature dependent sheet conductance

At low temperature due to weak thermal agitation, electrons are able to move longer distance (on an average) in it's trajectory with maintaining phase coherence which is known as phase coherence length (l_ϕ). Quantum interference manifests prominently when phase coherence length is very much longer than mean free path (l_e) of

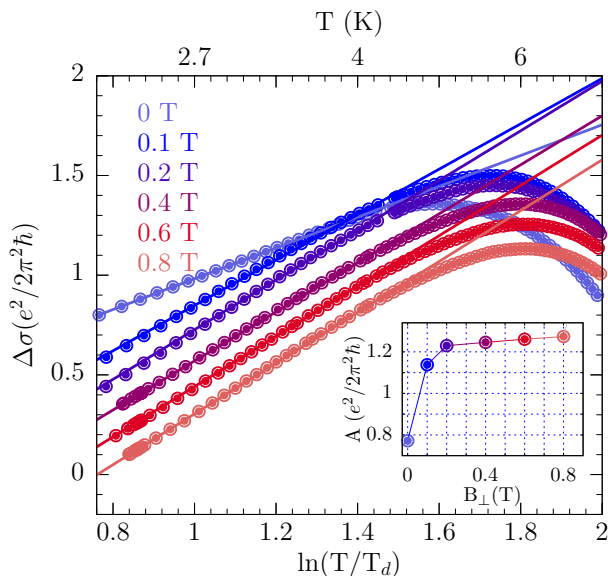


FIG. 2. Sheet conductance (relative change) $\Delta\sigma(T)$ vs $\ln(T/T_d)$ is plotted at different constant perpendicular magnetic fields ($0 \leq B_{\perp} \leq 0.8$ T) for Pt 16 nm thick film. Solid lines represent the fitting of $\Delta\sigma(T)$ vs $\ln(T/T_d)$ using Eq.(4) in the low temperature regime. (The upper x-axis denotes the real temperature and $T_d = 1$ K⁴¹) (vertically offset to plots are given for clarity). The extracted coefficient A for different B_{\perp} is shown in the inset.

electrons ($l_{\phi} \gg l_e$). One of the indications of quantum interference correction is $\ln(T)$ dependence of sheet conductance ($\Delta\sigma_{QI}$) in 2D limit ($l_{\phi} > t$, where t is film thickness) and in general, for N independent conducting channels or Fermi sheets, $\Delta\sigma_{QI}$ can be expressed as⁴²⁻⁴⁴,

$$\Delta\sigma_{QI}(T) = N\gamma_{int}\alpha p \frac{e^2}{2\pi^2\hbar} \ln(T/T_0) \quad (2)$$

where γ_{int} is related with interaction coupling strength among independent Fermi sheets (strong coupling and zero coupling lead to $N\gamma_{int} \sim 1$ and $N\gamma_{int} \sim N$ respectively), p is related with temperature exponent of phase coherence length ($l_{\phi}^2 \propto T^{-p}$ ⁴⁵⁻⁴⁷), T_0 depends on l_e and α takes different values depending upon dominant scattering process involved. For three extreme situations α follows as: $\alpha \sim -1/2$ in strong spin-orbit scattering with absence of magnetic impurity scattering (WAL), $\alpha \sim 1$ in quantum coherent regime ($l_{\phi} > l_e$) in absence of spin-orbit and magnetic impurity scattering (WL), $\alpha \sim 0$ in strong magnetic impurity scattering (which drives towards classical scenario)⁴². Therefore, the coefficient of $\ln(T)$ in Eq.(2), $A_{QI} = N\gamma_{int}\alpha p \frac{e^2}{2\pi^2\hbar}$ contains crucial information about microscopic scattering process. Further, EEI contribution to sheet conductance ($\Delta\sigma_e$) exhibits also similar $\ln(T)$ dependence. For N independent

channels in 2D limit, it can be expressed as⁴⁸⁻⁵²,

$$\Delta\sigma_e(T) = N \frac{e^2}{2\pi^2\hbar} (2 - 2F) \ln(T/T_e) \quad (3)$$

where F is averaged screened Coulomb interaction over Fermi surface, normalized with zero momentum transfer in EEI scattering process. Therefore, total correction to (σ_{total}) can be expressed as,

$$\Delta\sigma_{total}(T) = A \frac{e^2}{2\pi^2\hbar} \ln(T/T') \quad (4)$$

where $A = N(\gamma_{int}\alpha p + (2 - 2F))$ and T' is a constant.

Hence, it is not straight forward to extract the value of α from zero magnetic field $\Delta\sigma(T)$ vs $\ln(T)$ experimental data, when the contribution from quantum interference and EEI coexist. To overcome this issue, one needs to exploit the temperature dependence of sheet conductance at constant weak magnetic fields since it will suppress mainly quantum interference contribution.

Quantum interference effect (WL/WAL) originates from particle-particle channel interaction between two electrons traversing in ‘‘Cooperon loop’’ (CL) and it is very much sensitive to enclosed magnetic flux through the CL due to applied external magnetic field. However, EEI effect is governed by particle-hole channel interaction and it can not be influenced by external weak magnetic field⁴⁸ (EEI can be influenced in higher magnetic field if $g\mu_B B > 1/\tau_{so}$, where τ_{so} , g and μ_B are SOI scattering time, Lande-g factor and Bohr-magneton respectively)^{43,52-56}. As a consequence of the above fundamental differences between quantum interference effect (WL/WAL) and EEI, one can disentangle WL/WAL and EEI contribution by applying (perpendicular to film surface) constant weak external magnetic fields. The applied field will suppress WL/WAL contribution, while EEI effect remains unaffected. Hence, the change in $\ln(T)$ coefficient upon the application of weak magnetic field will provide only WL/WAL contribution (*i.e.* A_{QI} in Eq.(2)).

We investigated the variation of $\ln(T)$ coefficient (A) in $\sigma(T)$ with applying constant perpendicular external magnetic fields ranging from 0 - 0.8 T, shown in Fig.2. A systematic change in A was observed with the increment of external constant magnetic field and we obtained maximum change in $\ln(T)$ coefficient as $A_{QI} = A|_{B=0} - A|_{B=0.8} = -0.56$ (in quantum conductance unit, $e^2/2\pi^2\hbar$). To evaluate the value of α from A_{QI} that contains the information about dominant scattering process, one requires to know the values of $N\gamma_{int}$ and p . The p adapts a universal value depending upon the dominant interaction responsible for inelastic scattering process in the system. In particular, for EEI originated inelastic scattering, l_{ϕ}^{-2} ($l_{\phi}^2 \propto T^p$) exhibits linear temperature dependence at low-temperature and it shows a crossover from T to $T^2 \ln(T)$ behavior with the increment of temperature⁴⁷.

Two possible cases can be invoked to assess the value of α : (i) For Pt thin films, resistivity follows quadratic

temperature dependence ($14 \text{ K} < T < 23 \text{ K}$) (Sec:III) which signifies the dominance of electron-electron scattering over electron-phonon scattering and gives rise to $p = 1$ at lower temperature. Considering single channel $N = 1$ or strong coupling interaction $N\gamma_{int} \sim 1$, one can obtain $\alpha \sim -1/2$ (Eq.2). (ii) Effective two independent channels $N = 2$ and $p = 1$ (extracted from magnetoconductance analysis, Sec:V A) give rise to $\alpha \sim -0.28$ (Eq.2).

From detailed magnetotransport analysis (discussed in Sec:V), it is realized that the conduction takes place through two independent channels $N = 2$ in Pt thin films. Considering two channel conduction, Eq.2 provides the value of $\alpha = -0.56/(N\gamma_{int}p) = -0.56/(2 \times 1) \sim -0.28$ (as discussed above) which is very much unexpected for high spin-orbit coupled system. To find out the source of this discrepancy, we re-looked into how the explicit temperature dependence arises in the sheet conductance correction (Eq.2) due to quantum interference effect. One can primarily visualize that with the increment of temperature, random thermal agitation enhances the inelastic scattering among itinerant electrons and as a consequence, l_ϕ becomes temperature dependent (explicit functional form is determined by the dominating scattering mechanism (e - e , e -phonon scattering) at non zero temperature). The l_ϕ fixes the upper cut-off spatial dimension for quantum interference effect and the interference originated correction is proportional to the available coherence area ($\propto l_\phi^2$). Thus, for single channel with phase coherence length l_ϕ , $\Delta\sigma_{QI} \propto -\ln(l_\phi^2/l_e^2)$. On the contrary, dominant impurity induced inelastic scattering leads to temperature independent l_ϕ ⁵⁷ and such kind of conducting channel can not contribute to $\Delta\sigma_{QI}(T)$ considerably. Therefore, for a system with N non-similar independent conduction channel, $\Delta\sigma_{QI}(T)$ can be expressed as,

$$\Delta\sigma_{QI}(T) = -\alpha \sum_{n=1}^N \frac{e^2}{2\pi^2\hbar} \ln((l_\phi^n/l_e^n)^2). \quad (5)$$

It has been observed from magnetoconductance analysis that the examined Pt thin films possesses two independent conducting channels, one of which shows prominent temperature dependence ($B_\phi^1(T) \propto T$, Fig.3) at lower temperature regime ($2 \text{ K} < T < 6 \text{ K}$), and $B_\phi^2(T)$ associated with other channel follows a negligible variation with temperature. This implies that contribution to the slope of $\ln(T)$ (Eq.5) from second channel is negligible. Thus, Eq.5 can effectively be converted into

$$\begin{aligned} \Delta\sigma_{QI}(T) &= -\alpha \frac{e^2}{2\pi^2\hbar} \left(\ln(l_\phi^1/l_e^1)^2 + \ln(l_\phi^2/l_e^2)^2 \right) \\ &= -\alpha \frac{e^2}{2\pi^2\hbar} \left(\ln(l_\phi^1(T)/l_e^1)^2 + \ln(l_\phi^2(T)/l_e^2)^2 \right) \\ &\sim \alpha \frac{e^2}{2\pi^2\hbar} \left(\ln(T/T_0^1) + c \right) \end{aligned} \quad (6)$$

where, c is a temperature independent constant as l_ϕ^2 exhibits negligible temperature dependence. Since only one channel contributes logarithmic temperature correction to $\Delta\sigma_{QI}(T)$, we obtained $\alpha = -0.56/(N\gamma_{int}p) = -0.56/(1 \times 1) \sim -1/2$ which is consistent with theoretical value of α in presence of strong spin-orbit scattering.

We now turn into the estimation EEI strength which is related with screened Coulomb potential F . For strong interaction, F is small fractional number and for free electrons $F \sim 1$. F can be evaluated by considering that at a magnetic field of 0.8 T , the quantum interference effect is completely exhausted and then one can approximate the coefficient $A|_{B=0.8\text{T}} \sim N \times 2(1 - F) = 1.22$, ($N = 2$ as discussed before) which leads to $F \sim 0.7$. The $5d$ correlated transition metal Pt exhibits higher value of F which indicates e - e Coulomb interaction is weaker in comparison with strongly electron correlated $3d$ transition metal Cu $F_{Cu} \sim 0.5$ ⁵⁸.

V. WAL Effect from Magnetic field Variation

A. Perpendicular Magnetic field (B_\perp)

The magnetotransport measurement is a powerful tool to extract different types of microscopic scattering lengths (*i.e.* spin-orbit, inelastic scattering) by exploiting the quantum interference originated correction (WAL/WL) to sheet conductance. Quantum interference effect (WL/WAL) manifests more prominently with the reduction of dimension. For quasi-2D system (where phase coherent length (l_ϕ) is greater than film thickness (t)) with N independent conducting channels, the variation of sheet conductance ($\Delta\sigma(B_\perp) = \sigma(B_\perp) - \sigma(0)$) with external perpendicular magnetic field (B_\perp) is described by Hikami-Larkin-Nagaoka (HLN) equation which can be expressed as^{42,52,59-61},

$$\begin{aligned} \Delta\sigma(B_\perp) &= -\frac{e^2}{2\pi^2\hbar} \sum_{n=1}^N \left[\left\{ \psi(1/2 + B_e^n/B_\perp) + \ln(B_\perp/B_e^n) \right\} \right. \\ &\quad + \frac{1}{2} \left\{ \psi(1/2 + B_\phi^n/B_\perp) + \ln(B_\perp/B_\phi^n) \right\} \\ &\quad \left. - \frac{3}{2} \left\{ \psi(1/2 + \frac{B_\phi^n + B_{so}^n}{B_\perp}) + \ln\left(\frac{B_\perp}{B_\phi^n + B_{so}^n}\right) \right\} \right] \end{aligned} \quad (7)$$

where $\psi(x)$ is the digamma function, B_e^n , B_ϕ^n and B_{so}^n correspond to characteristic magnetic fields of n th channel which is related with scattering lengths (l_e , l_ϕ and l_{so}) as $B_i = \hbar/4el_i^2$, where l_e , l_ϕ and l_{so} denote elastic, phase coherence and spin-orbit scattering lengths respectively and B_e is determined from semi-classical approximation and detailed discussion is given in supplemental material⁶².

If independent channels are very much similar to each other, then the characteristic magnetic fields B_i^n corre-

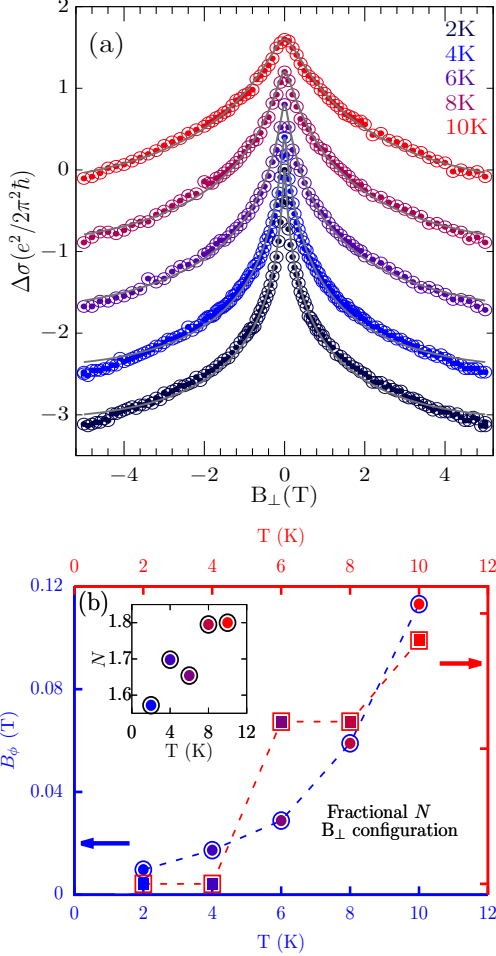


FIG. 3. (a) Magnetoconductance $\Delta\sigma(B_{\perp})$ is fitted with HLN equation at different temperature for 16 nm Pt film (solid gray color lines represent fitting of Eq.(8)) (vertically offset to plots are given for clarity). (b) Extracted B_{ϕ} B_{so} are illustrated at different temperatures, inset displays the fractional value of N at various temperatures.

sponding to each channel are nearly equal and as a result HLN Eq.(7) for N channels becomes

$$\begin{aligned} \Delta\sigma(B_{\perp}) = & -N \frac{e^2}{2\pi^2\hbar} \left[\left\{ \psi(1/2 + B_e/B_{\perp}) + \ln(B_{\perp}/B_e) \right\} \right. \\ & + \frac{1}{2} \left\{ \psi(1/2 + B_{\phi}/B_{\perp}) + \ln(B_{\perp}/B_{\phi}) \right\} \\ & \left. - \frac{3}{2} \left\{ \psi(1/2 + \frac{B_{\phi} + B_{so}}{B_{\perp}}) + \ln\left(\frac{B_{\perp}}{B_{\phi} + B_{so}}\right) \right\} \right]. \end{aligned} \quad (8)$$

Fig.3(a) shows the sheet conductance variation with perpendicular magnetic field for 16 nm thick film at different temperature. The presence of sharp cusp at lower temperature indicates the WAL effect. However, the sharpness disappears rapidly with the increment of tem-

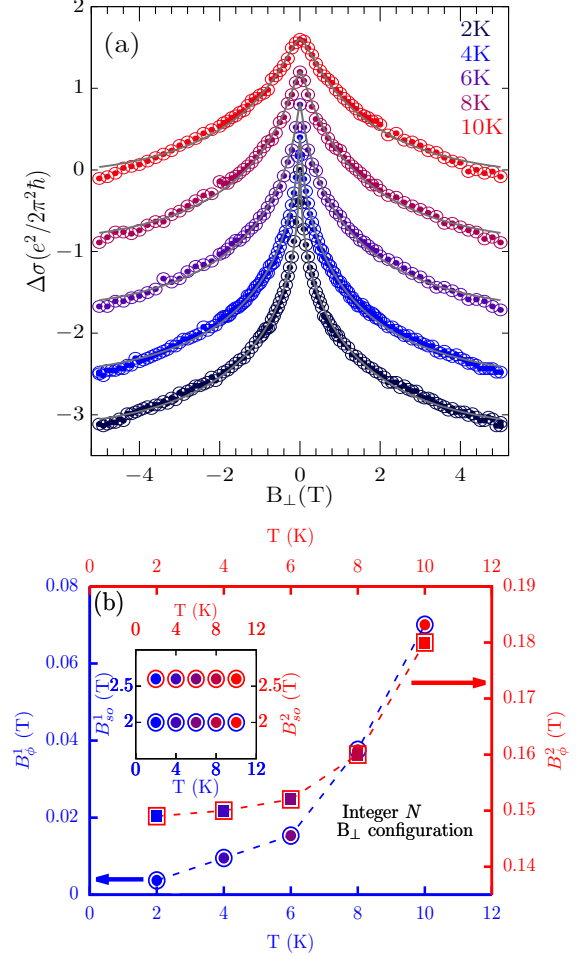


FIG. 4. (a) Magnetoconductance $\Delta\sigma(B_{\perp})$ is fitted with HLN equation at different temperature (solid gray color lines represent fitting of Eq.(7)) for 16 nm Pt film (vertically offset to plots are given for clarity). (b) Extracted B_{ϕ}^n for two different independent channels ($n = 1, 2$) are illustrated at different temperatures, inset displays the value of B_{so}^n at various temperatures.

perature. Experimental data $\Delta\sigma(B_{\perp})$ are fitted well with Eq.(8), nevertheless the fitting provides fractional value of N which can not be anticipated by considering independent conducting channels. The fitting and their corresponding best fitting parameters (B_{ϕ} , B_{so} , N) are illustrated in Fig.3(a) and 3(b) respectively. The fractional value of N can appear due to following reasons, (i) presence of weak but non-negligible inter-orbital scattering among channels^{63,64} and (ii) channels possess different set of B_e^n , B_{so}^n , B_{ϕ}^n .

To obtain more meaningful insight about the conducting channels in Pt thin films, the magnetoconductance data is further analyzed by considering more general equation (Eq.7) with the independent channels having different set of B_e^n , B_{so}^n , B_{ϕ}^n . The fitting is shown in Fig.4(a) and the best fitting parameters

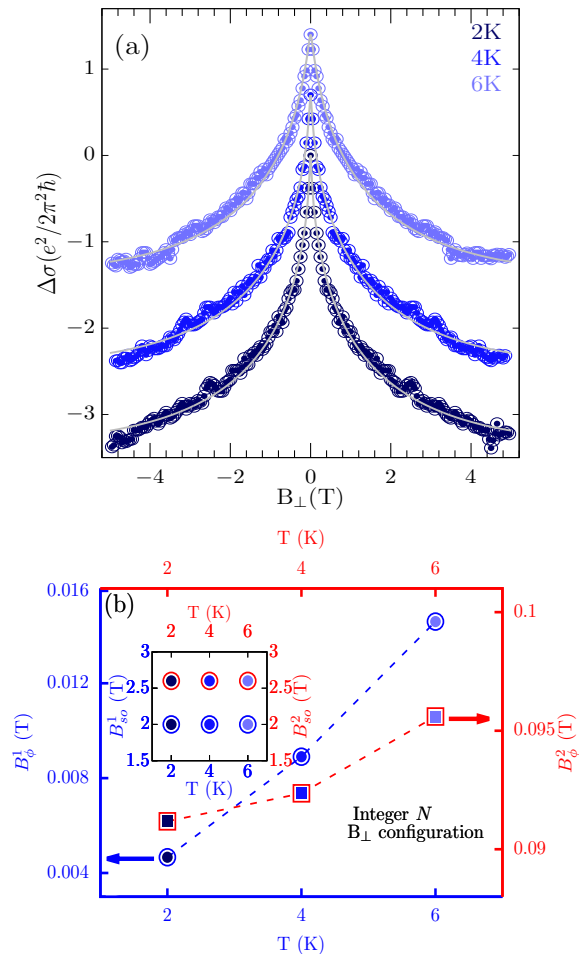


FIG. 5. (a) Magnetoconductance $\Delta\sigma(B_{\perp})$ is fitted with HLN equation at different temperature (solid gray color lines represent fitting of Eq.(7)) for 23 nm Pt film (vertically offset to plots are given for clarity). (b) Extracted B_{ϕ}^n for two different independent channels ($n = 1, 2$) are illustrated at different temperature, inset displays the value of B_{so}^n at various temperatures.

$(B_{\phi}^1, B_{\phi}^2, B_{so}^1, B_{so}^2)$ are shown in Fig.4(b) (for 16 nm thick Pt film). From the fitting, we obtain $N = 2$ and the phase coherence magnetic field ($B_{\phi}^1 \sim 0.004$ T at 2 K) for one channel to be higher than other ($B_{\phi}^2 \sim 0.15$ T at 2 K). Further, spin-orbit scattering magnetic field $B_{so}^1 \sim 2$ T, $B_{so}^2 \sim 2.5$ T are found to be very much higher than both B_{ϕ}^1, B_{ϕ}^2 . The obtained fitting parameters provide the following physical interpretations: (i) the Pt metal possesses large intrinsic spin-orbit interaction $B_{so} \sim 2$ T (in perpendicular configuration with integer number channels $N = 2$), (ii) presence of two independent conducting channels in Pt thin film, and (iii) the variation of B_{ϕ}^1 with temperature is very much prominent in comparison with the B_{ϕ}^2 and $B_{\phi}^1 < B_{\phi}^2$. The prominent variation of B_{ϕ}^1 vs T for one channel indicates that the inelastic scat-

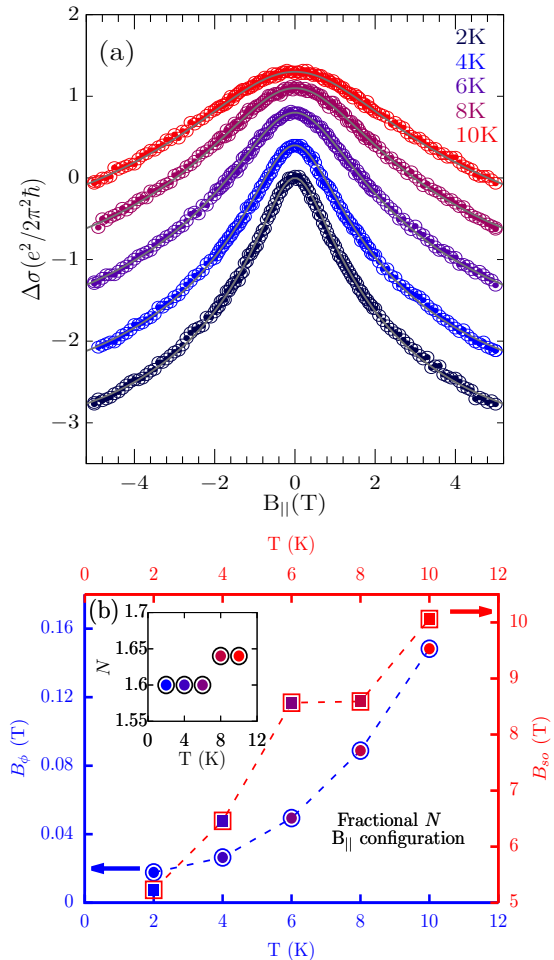


FIG. 6. (a) Magnetoconductance $\Delta\sigma(B_{\parallel})$ is fitted with HLN equation at different temperatures for 16 nm Pt film (solid gray color lines represent fitting of Eq.(8)) (vertically offset to plots are given for clarity). (b) Extracted B_{ϕ} B_{so} are illustrated at different temperature, inset displays the fractional value of N at various temperatures.

tering process is dominated by e - e scattering (Sec:III). However, the other channel with weakly temperature dependent inelastic scattering process (at low temperature regime $2 < T < 6$ K) indicates that significant amount of impurity scattering is present. To corroborate further, we analyzed the same for 23 nm thick Pt film and we found that it also follows similar behavior. The fitting and obtained parameters are illustrated in Fig.5(a), 5(b).

B. Parallel Magnetic field (B_{\parallel})

In quasi-2D system, itinerant electrons can diffuse along film thickness by satisfying the restriction of quantum mechanical boundary conditions⁵⁹. Hence, quan-

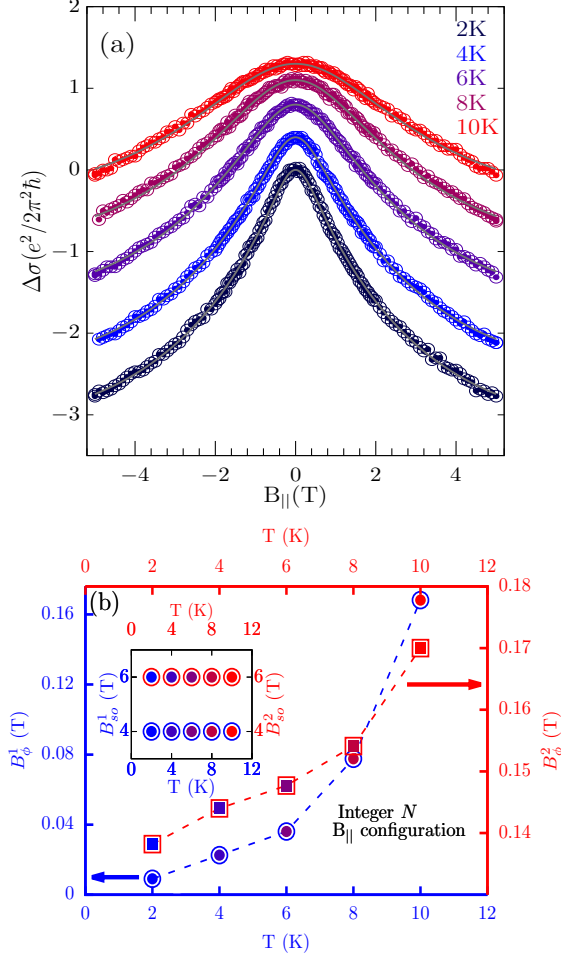


FIG. 7. (a) Magnetoconductance $\Delta\sigma(B_{||})$ is fitted with HLN equation at different temperatures (solid gray color lines represent fitting of Eq.(7)) for 16 nm Pt film (vertically offset to plots are given for clarity). (b) Extracted B_{ϕ}^n for two different independent channels ($n = 1, 2$) are illustrated at different temperatures, inset displays the value of B_{so}^n at various temperatures.

tum interference effect gets influenced even in parallel magnetic field configuration. Quantum interference originated magnetoconductance correction in $B_{||}$ configuration for N independent channels is given by^{44,59,65–67},

$$\Delta\sigma(B_{||}) = \frac{e^2}{2\pi^2\hbar} \sum_{n=1}^N \left[\frac{3}{2} \ln \left(1 + \frac{B_{||}^2}{B_t \cdot (B_{so}^n + B_{\phi}^n)} \right) - \frac{1}{2} \ln \left(1 + \frac{B_{||}^2}{B_t \cdot B_{\phi}^n} \right) \right] \quad (9)$$

where, B_t is defined as, $B_t = 12\hbar/et^2$ and t is film thickness.

For simplicity, if we assume all independent channels to have equal characteristic magnetic field then Eq.(9)

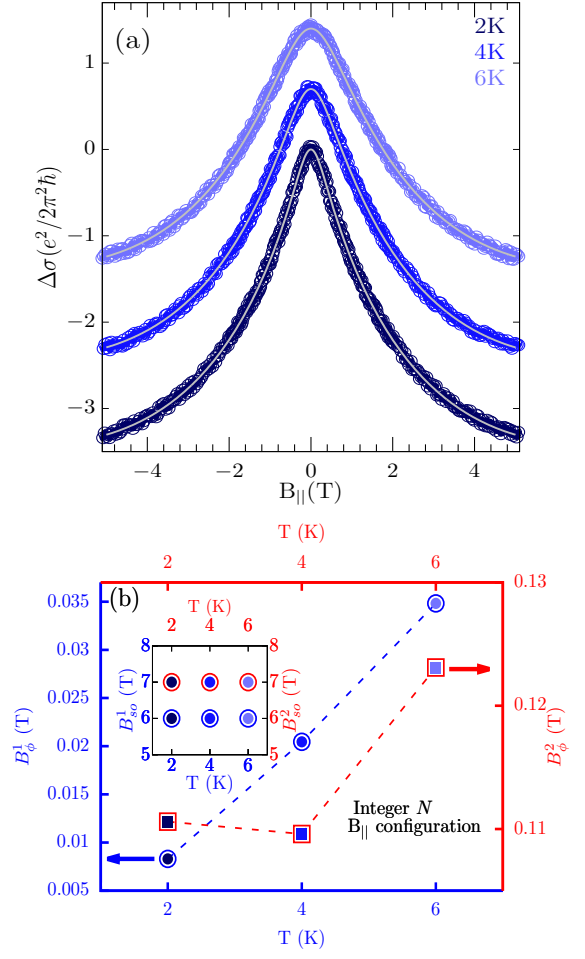


FIG. 8. (a) Magnetoconductance $\Delta\sigma(B_{||})$ is fitted with HLN equation at different temperatures (solid gray color lines represent fitting of Eq.(7)) for 23 nm Pt film (vertically offset to plots are given for clarity). (b) Extracted B_{ϕ}^n for two different independent channels ($n = 1, 2$) are illustrated at different temperatures, inset displays the value of B_{so}^n at various temperatures.

gets modified as

$$\Delta\sigma(B_{||}) = N \cdot \frac{e^2}{2\pi^2\hbar} \left[\frac{3}{2} \ln \left(1 + \frac{B_{||}^2}{B_t \cdot (B_{so} + B_{\phi})} \right) - \frac{1}{2} \ln \left(1 + \frac{B_{||}^2}{B_t \cdot B_{\phi}} \right) \right]. \quad (10)$$

Experimental data $\Delta\sigma(B_{||})$ are fitted well with Eq.(10) (Fig.6(a)), but the fitting provides fractional value of N . The extracted parameters are illustrated in Fig.6(b) for 16 nm thick film. As, previously we have discussed that number of independent conducting channel can not be a fractional value, different channels must have different characteristic magnetic fields. Therefore, we analyzed $\Delta\sigma(B_{||})$ considering the independent channels to have different set of B_{so}^n, B_{ϕ}^n (Eq.(9)) which is shown in

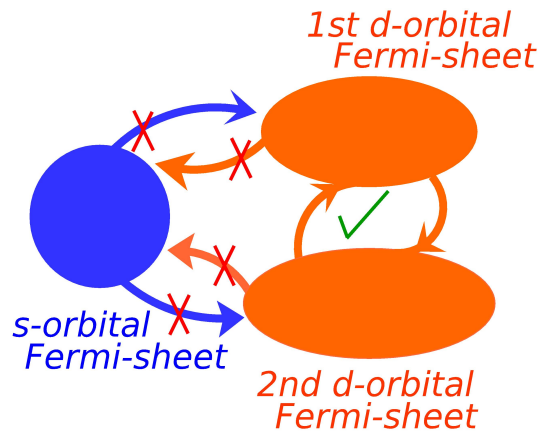


FIG. 9. The schematic diagram for theoretically predicated three Fermi-sheets one derived from s -orbital (blue color) and other two derived d -orbital (orange color). The possible interaction among them is denoted by arrows (allowed and forbidden interaction is marked by \times , \checkmark respectively). Interconnected two d -orbitals leads to one effective conducting channel and other one is from s -orbitals

Fig.7.(a) (for 16 nm thick Pt film), Fig.8.(a) (for 23 nm thick Pt film) and the best fitting parameters are shown in Fig.7.(b) (for 16 nm thick Pt film), Fig.8 (b) (for 23 nm thick Pt film)

In parallel magnetic field configuration, the extracted values of B_ϕ^1 (by fitting with Eq.9) are found to be petty close to B_ϕ^1 obtained (by fitting with Eq.7) in perpendicular magnetic field configuration and follows very much similar behaviour with temperature. However, the obtained B_{so} are very much different for perpendicular and parallel configuration. It confirms the anisotropic nature of the spin-orbit scattering potential in Pt thin films.

VI. Summary and Conclusions

It was predicted from a theoretical band structure calculation that Pt metal (electronic configuration $5d^96s^1$) has three sheets of Fermi surfaces which are comprised of s -band and two from d -band³⁴. We realised the pres-

ence of two independent conduction channels from our magneto-transport analysis in both perpendicular and parallel magnetic configurations. This apparent discrepancy (theoretically three channels, experimentally two channels) leads to an insightful physics of Pt thin film in presence of weak disorder scattering which is unavoidable in real system. The two d -band channels are mixed up with each other due to their similar orbital nature and in presence of intermixing scattering, they will act as an equivalent single channel. On the contrary, intermixing scattering among s , d -band channels is very weak due to different orbital symmetry. As a result effectively there will be two independent conducting channels which is illustrated in Fig.9. Secondly, we have found that the characteristic magnetic field for coherence phase breaking scattering (B_ϕ^2) corresponding to one channel shows a weak temperature dependence and this intriguing phenomena could arise very often in a system with significant impurity scattering. However, B_ϕ^1 for other channel shows a prominent variation with temperature, indicating the the presence of effectively weak impurity scattering. The crucial point is that the same amount of disorder in a system can act differently for different conduction channels depending upon it's orbital symmetry. The bands derived from more anisotropic orbitals (*e.g.* d , p orbital) are very much sensitive to minute amount of disorder^{68,69} which can give rise to very high inelastic scattering in comparison to conducting channel made out of symmetric orbitals (*e.g.* s orbital). To conclude, the symmetry of orbitals involved in conducting channels, presence of EEI and anisotropic spin-orbit interaction are revealed from our magnetoconductance study in Pt thin films.

ACKNOWLEDGMENTS

SJ and DS acknowledge the financial support from Max Planck partner group. DS acknowledges the funding support from SERB, Govt. of India. SJ would like to thank R. Kumar for discussions.

* subhadip.j@iopb.res.in

† dsamal@iopb.res.in

¹ A. Fert, *Rev. Mod. Phys.* **80**, 1517 (2008).

² I. Žutić, J. Fabian, and S. Das Sarma, *Rev. Mod. Phys.* **76**, 323 (2004).

³ S. Datta and B. Das, *Applied Physics Letters* **56**, 665 (1990).

⁴ J. Ryu, S. Lee, K.-J. Lee, and B.-G. Park, *Advanced Materials* **32**, 1907148 (2020).

⁵ S. Wolf, D. Awschalom, R. Buhrman, J. Daughton, v. S. von Molnar, M. Roukes, A. Y. Chtchelkanova, and

D. Treger, *science* **294**, 1488 (2001).

⁶ J. Tian, S. Hong, I. Miotkowski, S. Datta, and Y. P. Chen, *Science advances* **3**, e1602531 (2017).

⁷ M. I. D'Yakonov and V. Perel, *Soviet Journal of Experimental and Theoretical Physics Letters* **13**, 467 (1971).

⁸ M. I. Dyakonov and V. Perel, *Physics Letters A* **35**, 459 (1971).

⁹ J. Sinova, S. O. Valenzuela, J. Wunderlich, C. H. Back, and T. Jungwirth, *Rev. Mod. Phys.* **87**, 1213 (2015).

¹⁰ L. Zhu, D. C. Ralph, and R. A. Buhrman, *Applied Physics Reviews* **8**, 031308 (2021).

- ¹¹ X. Han, C. Wan, and G. Yu, “Materials, physics, and devices of spin-orbit torque effect,” (2021).
- ¹² C. Song, R. Zhang, L. Liao, Y. Zhou, X. Zhou, R. Chen, Y. You, X. Chen, and F. Pan, *Progress in Materials Science* **118**, 100761 (2021).
- ¹³ A. Manchon, J. Zelezny, I. M. Miron, T. Jungwirth, J. Sinova, A. Thiaville, K. Garello, and P. Gambardella, *Rev. Mod. Phys.* **91**, 035004 (2019).
- ¹⁴ S. O. Valenzuela and M. Tinkham, *Nature* **442**, 176 (2006).
- ¹⁵ J. Wunderlich, B. Kaestner, J. Sinova, and T. Jungwirth, *Phys. Rev. Lett.* **94**, 047204 (2005).
- ¹⁶ A. Mellnik, J. Lee, A. Richardella, J. Grab, P. Mintun, M. H. Fischer, A. Vaezi, A. Manchon, E.-A. Kim, N. Samarth, *et al.*, *Nature* **511**, 449 (2014).
- ¹⁷ J. Puebla, J. Kim, K. Kondou, and Y. Otani, *Communications Materials* **1**, 1 (2020).
- ¹⁸ T. H. Dang, J. Hawecker, E. Rongione, G. Baez Flores, D. Q. To, J. C. Rojas-Sanchez, H. Nong, J. Mangeney, J. Tignon, F. Godel, S. Collin, P. Seneor, M. Bibes, A. Fert, M. Anane, J.-M. George, L. Vila, M. Cosset-Cheneau, D. Dolfi, R. Lebrun, P. Bortolotti, K. Belashchenko, S. Dhillon, and H. Jaffres, *Applied Physics Reviews* **7**, 041409 (2020).
- ¹⁹ L. Liu, C.-F. Pai, Y. Li, H. Tseng, D. Ralph, and R. Buhrman, *Science* **336**, 555 (2012).
- ²⁰ R. Meservey and P. M. Tedrow, *Phys. Rev. Lett.* **41**, 805 (1978).
- ²¹ A. Magni, V. Basso, A. Sola, G. Soares, N. Meggiato, M. Kuepferling, W. Skowroński, S. Lazarski, K. Grochot, M. V. Khanjani, J. Langer, and B. Ocker, *IEEE Transactions on Magnetics* **58**, 1 (2022).
- ²² G. Choi, J. Ryu, R. Thompson, J.-G. Choi, J. Jeong, S. Lee, M.-G. Kang, M. Kohda, J. Nitta, and B.-G. Park, *APL Materials* **10**, 011105 (2022).
- ²³ L. Chen, K. Zollner, S. Parzefall, J. Schmitt, M. Kronseder, J. Fabian, D. Weiss, and C. H. Back, *Phys. Rev. B* **105**, L020406 (2022).
- ²⁴ G. G. B. Flores and K. D. Belashchenko, *Phys. Rev. B* **105**, 054405 (2022).
- ²⁵ E. Saitoh, M. Ueda, H. Miyajima, and G. Tatara, *Applied Physics Letters* **88**, 182509 (2006).
- ²⁶ T. Kimura, Y. Otani, T. Sato, S. Takahashi, and S. Maekawa, *Phys. Rev. Lett.* **98**, 156601 (2007).
- ²⁷ G. Bergmann, *International Journal of Modern Physics B* **24**, 2015 (2010).
- ²⁸ J. Rammer, *Quantum Field Theory of Non-Equilibrium States* (Cambridge University Press, 2011).
- ²⁹ P. Coleman, *Introduction to Many-Body Physics* (Cambridge University Press, 2015).
- ³⁰ G. Bergmann, *Physics Reports* **107**, 1 (1984).
- ³¹ F. V. Tikhonenko, A. A. Kozikov, A. K. Savchenko, and R. V. Gorbachev, *Phys. Rev. Lett.* **103**, 226801 (2009).
- ³² G. Bergman, *Phys. Rev. Lett.* **48**, 1046 (1982).
- ³³ E. McCann, *Physics* **2**, 98 (2009).
- ³⁴ L. R. Windmiller, J. B. Ketterson, and S. Hornfeldt, *Journal of Applied Physics* **40**, 1291 (1969).
- ³⁵ J. B. Ketterson and L. R. Windmiller, *Phys. Rev. B* **2**, 4813 (1970).
- ³⁶ G. Y. Guo, S. Murakami, T.-W. Chen, and N. Nagaosa, *Phys. Rev. Lett.* **100**, 096401 (2008).
- ³⁷ W. De Haas and J. De Boer, *Physica* **1**, 609 (1934).
- ³⁸ M. J. Rice, *Phys. Rev. Lett.* **20**, 1439 (1968).
- ³⁹ A. Jacko, J. Fjaerestad, and B. Powell, *Nature Physics* **5**, 422 (2009).
- ⁴⁰ X. Lin, B. Fauqué, and K. Behnia, *Science* **349**, 945 (2015).
- ⁴¹ Function $\ln(x)$ is not defined for dimensioned quantities. Therefore, to make the argument dimensionless, we use $\ln(T/T_d)$ as the x-axis label of Fig.2 with $T_d = 1$ K.
- ⁴² S. Hikami, A. I. Larkin, and Y. Nagaoka, *Progress of Theoretical Physics* **63**, 707 (1980).
- ⁴³ P. A. Lee and T. V. Ramakrishnan, *Rev. Mod. Phys.* **57**, 287 (1985).
- ⁴⁴ N. P. Breznay, H. Volker, A. Palevski, R. Mazzarello, A. Kapitulnik, and M. Wuttig, *Phys. Rev. B* **86**, 205302 (2012).
- ⁴⁵ B. L. Altshuler, A. G. Aronov, and D. E. Khmel'nitsky, *Journal of Physics C: Solid State Physics* **15**, 7367 (1982).
- ⁴⁶ H. Fukuyama and E. Abrahams, *Phys. Rev. B* **27**, 5976 (1983).
- ⁴⁷ B. N. Narozhny, G. Zala, and I. L. Aleiner, *Phys. Rev. B* **65**, 180202 (2002).
- ⁴⁸ B. L. Altshuler, A. G. Aronov, and P. A. Lee, *Phys. Rev. Lett.* **44**, 1288 (1980).
- ⁴⁹ H. Fukuyama, *Journal of the Physical Society of Japan* **50**, 3407 (1981).
- ⁵⁰ H. Fukuyama, *Journal of the Physical Society of Japan* **51**, 1105 (1982).
- ⁵¹ H. Fukuyama, *Journal of the Physical Society of Japan* **50**, 3562 (1981).
- ⁵² S. Jana, T. Senapati, and D. Samal, *Phys. Rev. B* **103**, 245109 (2021).
- ⁵³ B. L. Altshuler, D. Khmel'nitskii, A. I. Larkin, and P. A. Lee, *Phys. Rev. B* **22**, 5142 (1980).
- ⁵⁴ P. A. Lee and T. V. Ramakrishnan, *Phys. Rev. B* **26**, 4009 (1982).
- ⁵⁵ P. Seiler, J. Zabaleta, R. Wanke, J. Mannhart, T. Kopp, and D. Braak, *Phys. Rev. B* **97**, 075136 (2018).
- ⁵⁶ A. Y. Kuntsevich, L. A. Morgun, and V. M. Pudalov, *Phys. Rev. B* **87**, 205406 (2013).
- ⁵⁷ K. Munakata, T. H. Geballe, and M. R. Beasley, *Phys. Rev. B* **84**, 161405 (2011).
- ⁵⁸ Y. Fehr, S. May-tal, and R. Rosenbaum, *Phys. Rev. B* **33**, 6631 (1986).
- ⁵⁹ B. Al'Tshuler and A. Aronov, *JETP Lett.*, **33**, 499 (1981).
- ⁶⁰ S. Jana, S. G. Bhat, B. C. Behera, L. Patra, P. S. A. Kumar, B. R. K. Nanda, and D. Samal, *EPL, Europhysics Letters*, **133**, 17005 (2021).
- ⁶¹ L. Zhang, M. Dolev, Q. I. Yang, R. H. Hammond, B. Zhou, A. Palevski, Y. Chen, and A. Kapitulnik, *Phys. Rev. B* **88**, 121103 (2013).
- ⁶² See Supplemental Materials:... for the estimation of B_e .
- ⁶³ Two extreme situations *i.e.* in presence (absence) of strong inter-orbital scattering among N channels gives rise to effective single channel (N channels) for magnetotransport phenomena. Therefore, intuitively non-integer value of independent channel may arise for intermediate (small but non-negligible) inter-orbital scattering strength.
- ⁶⁴ H. Nakamura, D. Huang, J. Merz, E. Khalaf, P. Ostrovsky, A. Yaresko, D. Samal, and H. Takagi, *Nature communications* **11**, 1 (2020).
- ⁶⁵ R. Rosenbaum, *Phys. Rev. B* **32**, 2190 (1985).
- ⁶⁶ R. S. Markiewicz and C. J. Rollins, *Phys. Rev. B* **29**, 735 (1984).
- ⁶⁷ W. C. McGinnis and P. M. Chaikin, *Phys. Rev. B* **32**, 6319 (1985).
- ⁶⁸ N. Mott, *Philosophical Magazine* **17**, 1259 (1968).
- ⁶⁹ N. F. Mott, *Philosophical Magazine* **19**, 835 (1969).